Electronic Supplementary Information

An "AND"-Logic-Gate Based Fluorescent Probe with Dual Reactive Sites for Monitoring Extracellular Methylglyoxal Level Changes of Activated Macrophages

Wenli Wang,[#a] Junwei Chen,[#a] Huijuan Ma,[#a] Wanjin Xing,[a] Nan Lv,[a] Baoning Zhang,[a] Huan Xu,[*a] Wei Wang,[*a,b] and Kaiyan Lou[*a]

[a] *State Key Laboratory of Bioengineering Reactor, Shanghai Key Laboratory of New Drug Design, and Shanghai Key Laboratory of Chemical Biology, School of Pharmacy, East China University of Science & Technology, 130 Meilong Road, Shanghai 200237, China.*
[b] *Department of Pharmacology and Toxicology and BIO5 Institute, University of Arizona, Tucson, AZ 85721-0207, United States.*

Table of Contents

General Information

Commercial reagents were purchased from commercial suppliers and used as received, unless otherwise stated.

^{1}H and ^{13}C NMR spectra were recorded on Bruke DRX 400 (400 MHz). Data for ^{1}H are reported as follows: chemical shift (ppm), and multiplicity (s = singlet, bs = broad singlet, d = doublet, t = triplet, q = quartet, m = multiplet). Data for ^{13}C NMR are reported as ppm. Mass Spectra were obtained from East China University of Science and Technology LC-Mass spectral facility. UV-Vis spectra were collected on a Shimadzu UV-1800 spectrophotometer. Fluorescence spectra were collected on a FluoroMax-4 (Horiba Scientific) fluorescence spectrophotometer with slit widths were set at 4 nm both for excitation and emission unless otherwise stated. The pH measurements were carried out with a FE20 plus (Mettler Toledo) pH meter.

Part I: Probe Design

1.1 Comparison structure of known fluorescent probes for MGO.

a) Fluorescent or phosphorescent probes for MGO containing a single irreversible reactive site

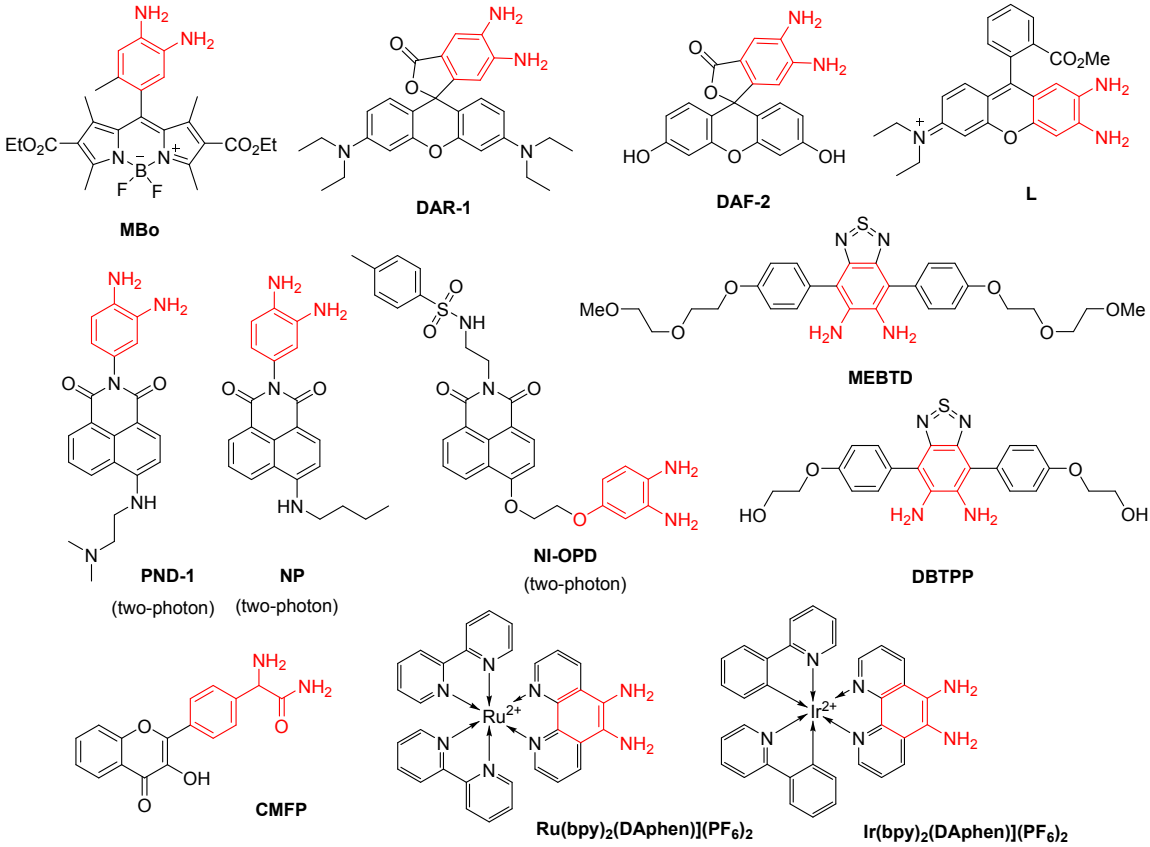

b) Fluorescent probes for MGO (and GO) with a single reversible reactive site

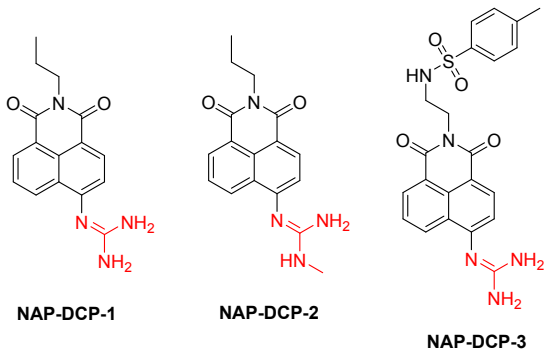

c) This work: Fluorescent probes for MGO (and GO) with both reversible and irreversible reactive site

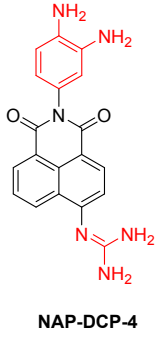

Figure S1 Structures of fluorescent probes for MGO.

1.2 Further illustration of the two reactive groups forming “AND” logic gate.

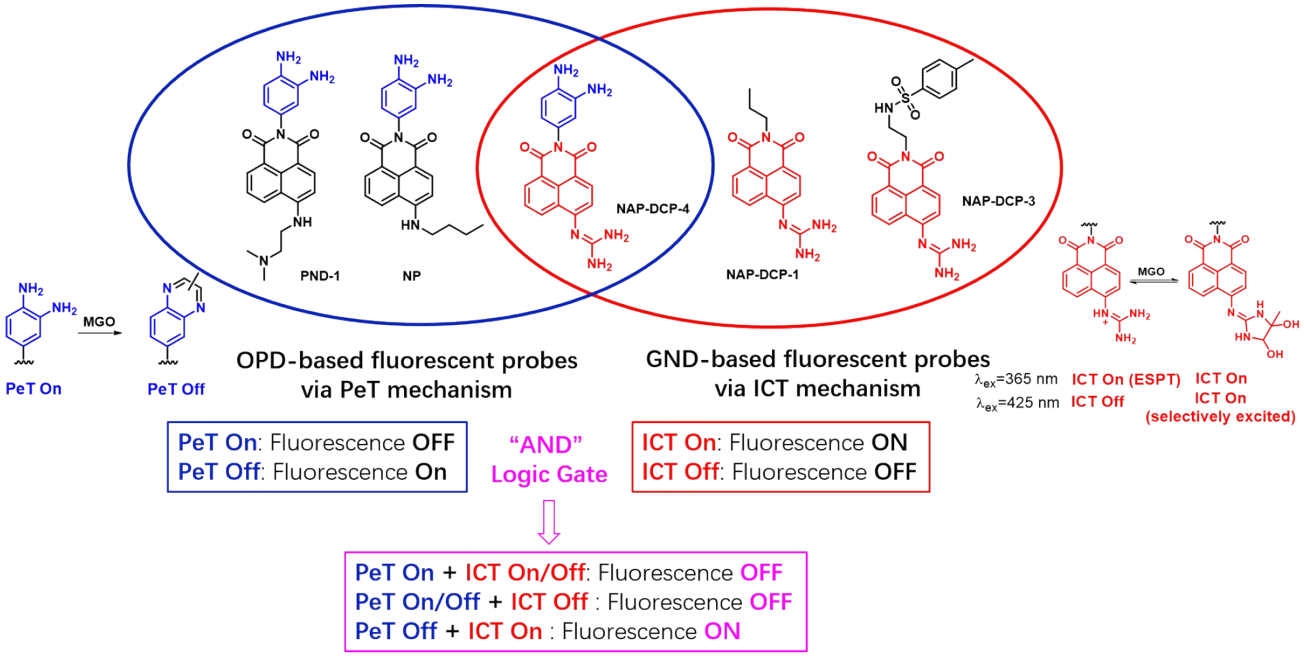

Figure S2 Venn Diagram of the OPD-based fluorescent probes for MGO via PeT mechanism and GND-based fluorescent probes for MGO and GO via ICT mechanism. The overall fluorescence responses of the probe **NAP-DCP-4** is the result of “AND” logic calculation of the fluorescence responses of the two reactive groups when they are used alone.

Table S1 Comparison of literature reported fluorescent probes for GOS.
(N. A. means the information "not available" from the literature)

Probe	Ex nm	Em nm	LOD for MGO μM	Optimized condition for MGO/GO detection	Ref.
CMFP	350	525↓440↑ (ratiometric)	0.24	10 μM probe + 500 μM MGO 90 min at 37°C in DMSO/PBS (1/9, v/v, 100 mM, pH 7.4).	1
NI-OPD	380 780 (TP)	460↑ (turn-on)	0.56 nM	10 μM probe + 30 μM MGO 2h at 37°C in DMF/PBS (1/9, v/v, 10 mM, pH 7.4)	2
NP	440 760 (TP)	550↑ (turn-on)	1.47	5 μM probe + 150 μM MGO 1 h in DMSO/PBS (1/19, v/v, pH 7.4)	3
PND-1	440 880 (TP)	528↑ (turn-on)	77 nM	5 μM probe + 50 μM MGO 12 h at 37°C in DMSO/PBS (1/9, v/v, 10 mM, pH 7.4)	4
MBo	480	532↑ (turn-on)	50-100 nM	10 μM probe + 50 μM MGO 1 h at 37 °C in PBS (pH 7.4) slit =1/10 nm	5
L	520	642↓ (turn-off)	N. A.	5 μM probe EtOH/tris-HCl buffer (3/7, v/v, 10 mM, pH 7.4) slit = 5/10 nm	6
DAF-2	435	510↑ (turn-on)	0.7	10 μM probe + 50 μM MGO 30 min at 37 °C in PBS (100 mM, pH 7.4)	7
DAR-1	545	570↑ (turn-on)	N. A.	10 μM probe + 50 μM MGO 30 min at 37 °C in PBS (100 mM, pH 7.4)	7
MEBTD	496	650	18 nM	50 μM probe + 50 μM MGO DMAC/PBS (2/3, v/v, 20 mM, pH 7.4)	8
DBTPP	550	650	0.262	25 μM probe+ 60 μM MGO 10 mM PBS (pH = 7.4, and 40% DMAC).	9
$Ru(bpy)_2(DAphen)](PF_6)_2$	450-490	612↑ (turn-on)	0.78	10 μM probe + 800 μM MGO 2h in EtOH/PBS (2/1, v/v, 25 mM, pH 7.4)	10
$Ir(bpy)_2(DAphen)](PF_6)_2$	450-490	605↑ (turn-on)	1.15	10 μM probe + 800 μM MGO 2h in EtOH/PBS (2/1, v/v, 25 mM, pH 7.4)	10
NAP-DCP-1	425	564↑ (turn-on)	0.72 (MGO), 0.58 (GO)	2 μM probe + 200 μM MGO 30 min at room temperature in PBS (10 mM, pH 7.4)	11
NAP-DCP-2	425	564↑	1.1	2 μM probe + 400 μM MGO 60 min at room temperature in PBS (10 mM, pH 7.4)	11
NAP-DCP-3	425	564	0.13 (MGO), 0.16 (GO)	2 μM probe + 200 μM MGO 30 min at room temperature in PBS (10 mM, pH 7.4)	11
NAP-DCP-4	425	559	2.2	2 μM probe + 200 μM MGO 1.5 h at 37 °C	This work

Part II Synthetic Procedures and Structural Characterizations:

2.1 Synthesis of NAP-DCP-4

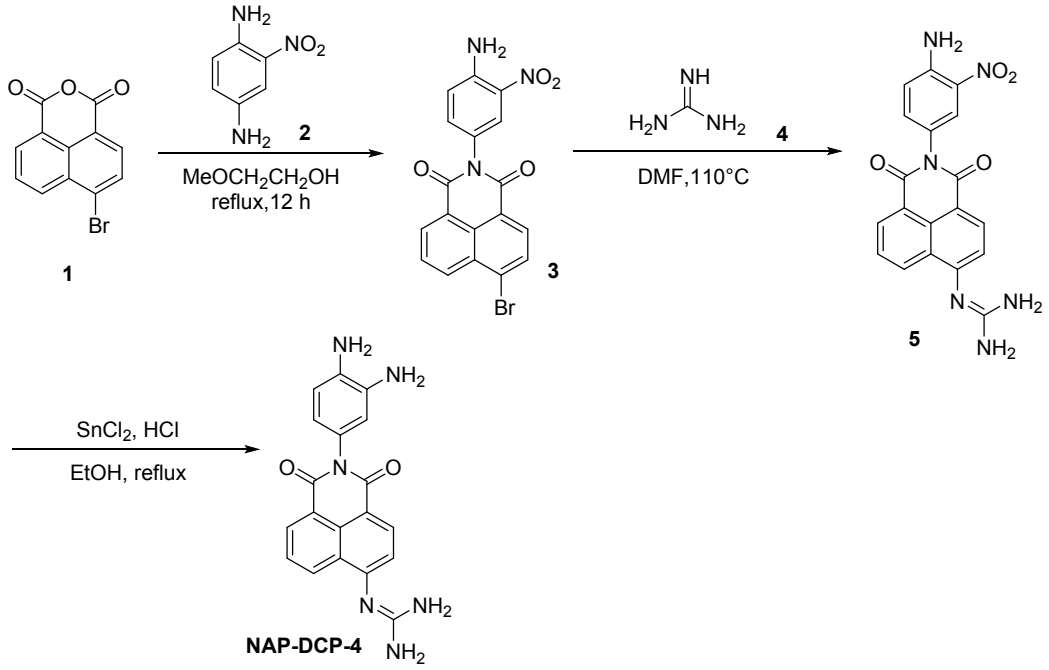

Scheme S1 Synthesis of the probe **NAP-DCP-4**

2-(*N*-4-amino-3-nitrophenyl)-6-bromo-1,8-naphthalimide (3)[12]

A mixture of 4-Bromo-1,8-naphthalic anhydride (500 mg, 1.80 mmol) and 1,4-diamino-2-nitrobenzene (550 mg, 3.59 mmol) was refluxed in 15 mL 2-methoxylethanol for 12 h. The reaction mixture was cooled to room temperature and yielded a precipitate. The precipitate was filtered to afford the pale yellow solid as the product (634.7 mg, 85.1%), which was directly used for the next step without purification.

2-(*N*-(4-amino-3-nitrophenyl)-1,8-naphthalimide-4-yl)guanidine (5)

To the bromide **3** (309 mg, 0.750 mmol) dissolved in 5 mL DMF was added dropwise a solution of guanidine (180 mg, 3.59 mmol) in 5 mL DMF. The reaction mixture was stirred at 110 °C for 4 h under nitrogen. After cooled to room temperature, the reaction mixture was poured into 200 mL ethyl acetate, and a brown precipitate was isolated by filtration. The resulting solid was purified by silica gel column chromatography using CH_2Cl_2/MeOH (v/v 10 : 1) as the eluent to afford the title compound **5** (179 mg, 60 %) as yellow solid. ^{1}H NMR (DMSO-d_6, 400 MHz) δ 8.60 (d, J = 8.4 Hz, 1H), 8.48 (d, J = 7.2 Hz, 1H), 8.36 (d, J = 8.1 Hz, 1H), 7.99 (d, J = 2.4 Hz, 1H), 7.80 (t, J = 7.8 Hz, 1H), 7.62 (bs, 2H); 7.43 (bd, J = 8.1 Hz, 1H), 7.38 (dd, J = 9.0, 2.4 Hz, 1H), 7.12 (d, J = 9.0 Hz, 1H), 6.83 (bs, 4H); ^{13}C NMR (not available due to its low solubility); ESI-HRMS: m/z $[M+H]^+$ calcd for $[C_{19}H_{15}N_6O_4]^+$ 391.1149, found 391.1156.

2-(*N*-(3,4-diaminophenyl)-1,8-naphthalimide-4-yl)guanidine (NAP-DCP-4)

To a suspension of the compound **5** (179 mg, 0.459 mmol) in ethanol (9 mL), was slowly added with a solution of $SnCl_2 \cdot 2H_2O$ (727 mg, 3.22 mmol) in 0.7 mL concentrated hydrochloric acid. The reaction mixture was refluxed for 3 h, cooled to room temperature, and then carefully neutralized with saturated $NaHCO_3$ aqueous solution until there were no further bubbles formed. The resulting mixture were extracted with ethyl acetate twice (100 mL ×2). The combined organic layers were dried over sodium sulfate, concentrated and purified by silica gel column chromatography using CH_2Cl_2/MeOH (v/v 7 : 1) as the eluent to afford the probe **NAP-DCP-4** (24.9 mg, yield: 15%) as yellow solid. ^{1}H NMR (DMSO-d_6, 400 MHz) δ 8.59 (d, J = 8.4 Hz, 1H), 8.42 (d, J = 7.3 Hz, 1H), 8.29 (d, J = 8.2 Hz, 1H), 7.71 (t, J = 7.8 Hz, 1H), 7.28 (d, J = 8.0 Hz, 1H), 6.57 (d, J = 8.1 Hz, 1H), 6.48 (s, 4H), 6.37 (d, J = 2.3 Hz, 1H), 6.25 (dd, J = 8.1, 2.3 Hz, 1H), 4.58 (s, 4H); ^{13}C NMR (400 MHz, DMSO-d_6) δ 164.3 (2C), 163.6, 156.0, 135.2, 134.8, 132.7, 130.8, 130.7, 129.7, 127.6, 127.6, 125.6, 125.1, 122.4, 118.1, 117.3, 114.8, 114.0; ESI-HRMS: m/z $[M+H]^+$ calcd for $[C_{19}H_{17}N_6O_2]^+$ 361.1408, found 361.1411.

Part III: Fluorescence and Absorption Spectroscopy Studies

3.1 Spectroscopic materials

All aqueous solutions were prepared using double distilled water. **NAP-DCP-4** stock solution (1 mM in dry DMSO) was prepared and stored at -20 °C. All fluorescence and absorption spectroscopic measurements were performed in 10 mM phosphate buffer (pH 7.4) at 25 °C unless otherwise stated. Samples for absorption and fluorescence measurements were contained in 1 cm×1 cm quartz cuvettes (3.5 mL volume).

3.2 Time-dependent absorption spectra of NAP-DCP-4 upon addition of 200 equiv. MGO or GO at pH 7.4.

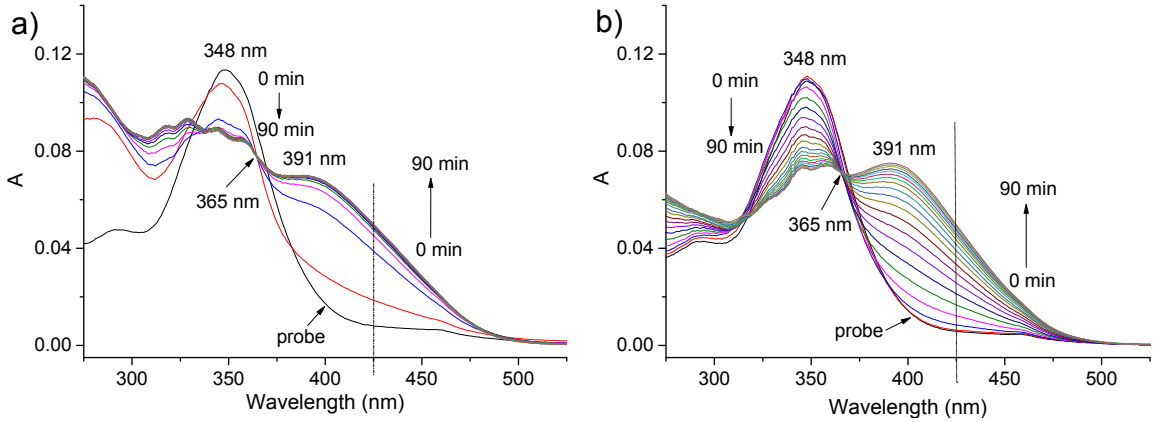

Figure S3 Time-dependent absorption spectra of **NAP-DCP-4** (10 μM) upon addition of 200 equiv. MGO (a) or GO (b). (Data were taken every 5 min in 10 mM PBS buffer solution at pH 7.4 at room temperature).

3.2 Time-dependent fluorescence emission spectra of NAP-DCP-4 upon addition of 100 equiv. MGO or GO at pH 7.4.

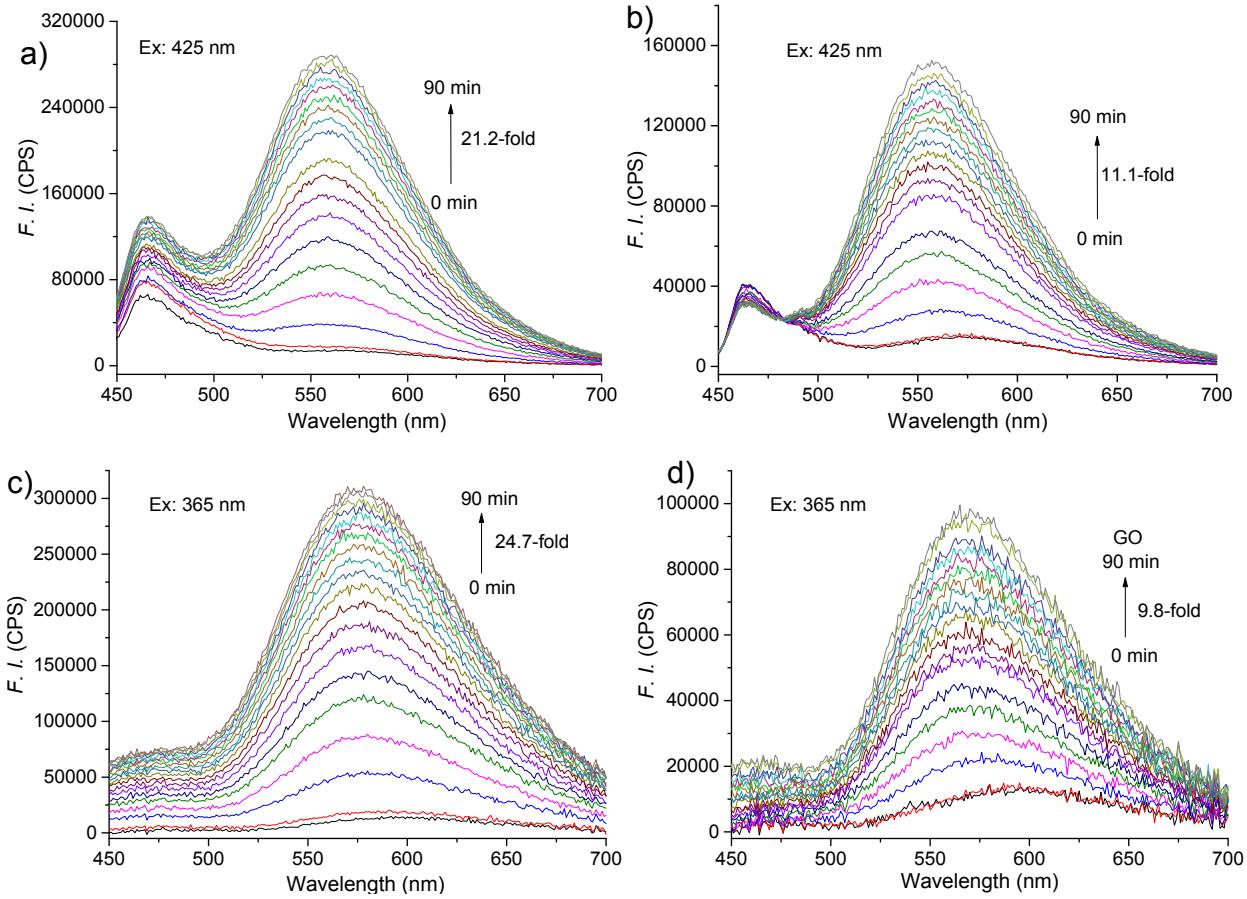

Figure S4 a-b) Time-dependent fluorescence emission spectra (λ_{ex} = 425 nm) of **NAP-DCP-4** (2 μM) upon addition of 100 equiv. MGO (a) or GO (b); c-d) Time-dependent fluorescence emission spectra (λ_{ex} = 365 nm) of **NAP-DCP-4** (2 μM) upon addition of 100 equiv. MGO (c) or GO (d) (Data were taken every 5 min in 10 mM PBS buffer solution at pH 7.4 at 37 °C).

3.3 Normalized fluorescence excitation and emission spectra of NAP-DCP-4 and the probe after incubation of 100 equiv. MGO at pH 7.4.

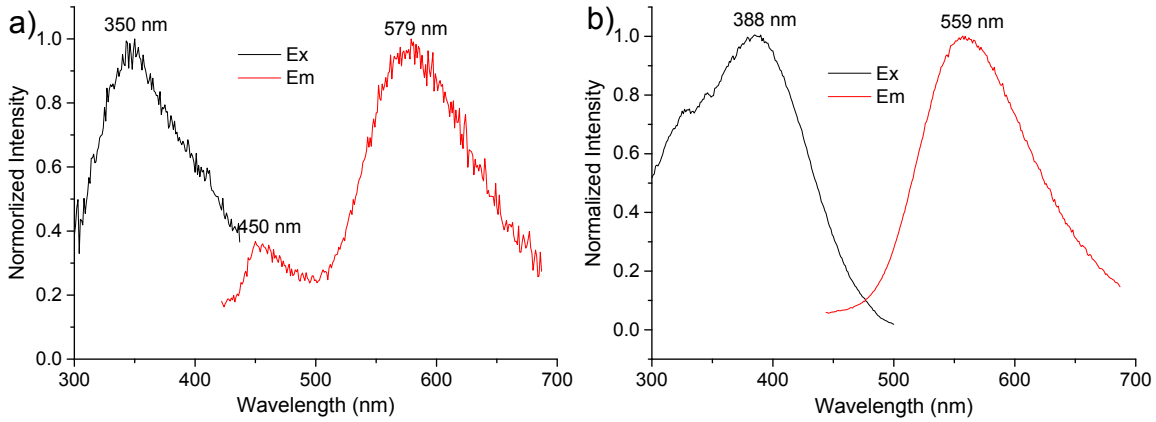

Figure S5 a) Normalized fluorescence excitation and emission spectra of the probe **NAP-DCP-4** (2 μM); b) Normalized fluorescence excitation and emission spectra of the probe **NAP-DCP-4** (2 μM)

upon incubation of MGO (200 μM) at 37 °C for 1.5 h.

3.4 Reversibility studies of the probe NAP-DCP-4 for GO

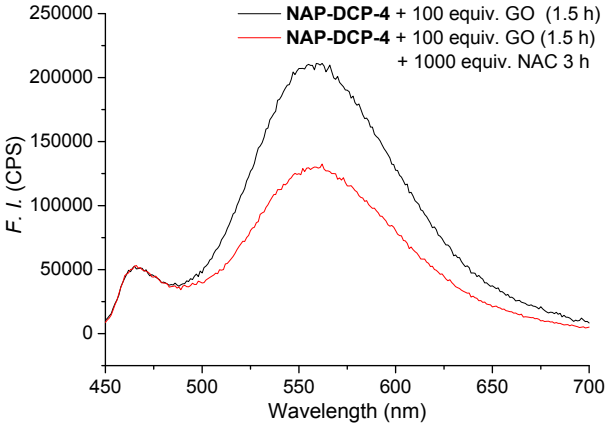

Figure S6 Fluorescence emission spectra of the probe **NAP-DCP-4** (2 μM) upon incubation with 100 equiv. GO at 37 °C versus further addition of 1000 equiv. NAC and then incubation for another 3 h at 37 °C.

3.5 Detection limits of NAP-DCP-4 for MGO without or in the presence of FA

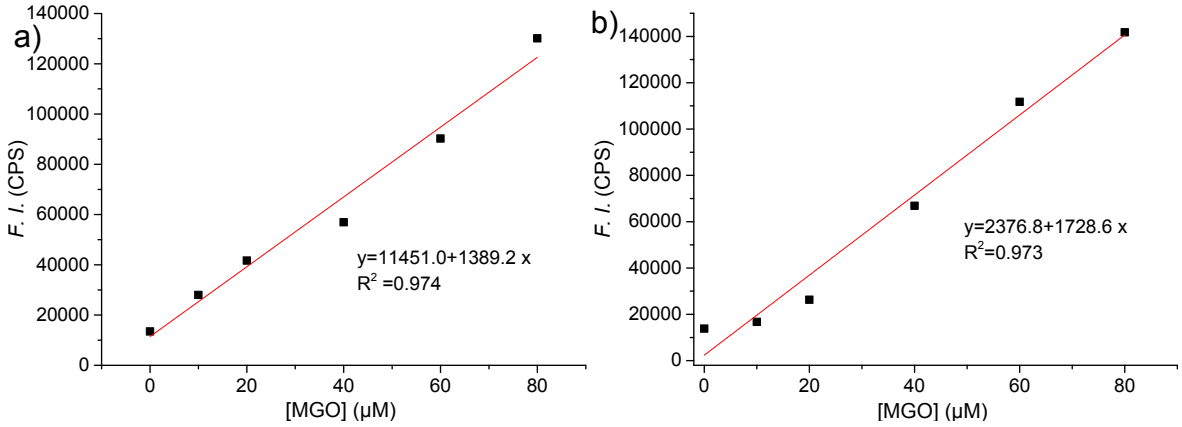

Figure S7 Fluorescence intensity of the probe **NAP-DCP-4** (2 μM) upon incubation with 0, 10, 20, 40, 60, 80 μM of MGO at 37 °C for 1.5 h without (a) or in the presence of 400 μM formaldehyde.

3.6 Selectivity studies of the probe NAP-DCP-4 for MGO detection under excitation 365 nm.

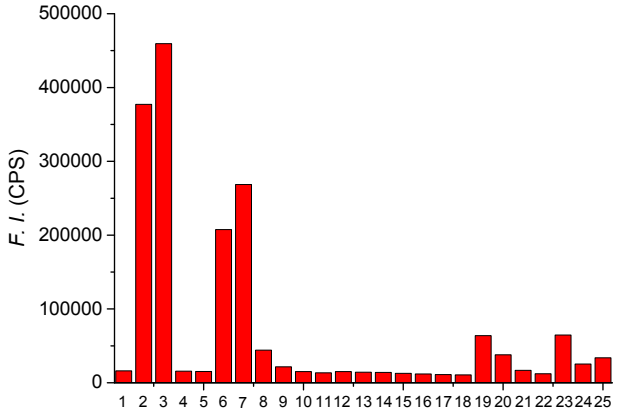

Figure S8 Fluorescence intensity at 564 nm (excited at 365 nm) of the probe **NAP-DCP-4** (2 μM) upon incubation with 100 equiv. of various other species. 1: probe only, 2: MGO, 3: MGO and 1000 equiv. FA, 4: FA, 5: acetaldehyde, 6: GO, 7: GO and 1000 equiv. FA, 8: *o*-phthalaldehyde, 9: glyoxylic acid, 10: benzaldehyde, 11 GSH, 12: glucose, 13: cysteine, 14: proline, 15: isoleucine, 16: H_2O_2, 17: K^+, 18: Na^+, 19: Cu^{2+}, 20: Zn^{2+}, 21: Al^{3+}, 22: Ca^{2+}, 23: Fe^{2+}, 24: Fe^{3+}, 25 NOC-18.

3.7 Time-dependent Fluorescence Spectra and UV-Vis Spectra Studies of NAP-DCP-4 for MGO in the presence of NO

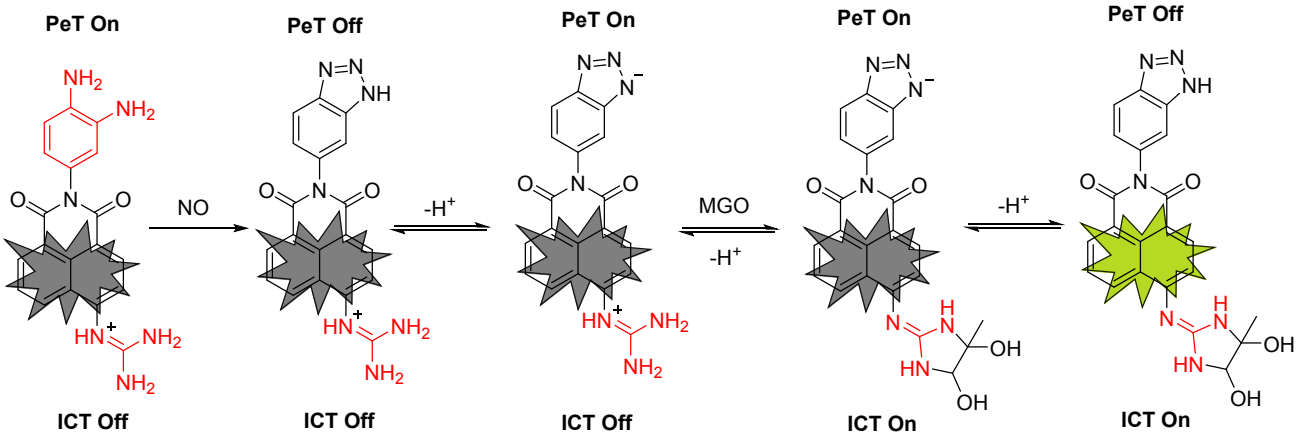

Scheme S2 Proposed low fluorescence turn-on ratio of the probe **NAP-DCP-4** for MGO in the presence of NO. (The OPD reactive site reacts with NO quickly and forms benzotriazole irreversibly, which deprotonates at pH 7.4. The benzotriazole anion formed functions as a fluorescence quenching group through PeT effect. From previous studies, it is known that NO does not interfere with the guanidino group's reaction with MGO to form exocyclic dihydroxyimidazolidines with reduced pKa. The deprotonated dihydroxyimidazolidines is selectively excited at 425 nm to generate fluorescence turn-on response when the benzotriazole is in its neutral form, which is only a small portion in equilibrium.)

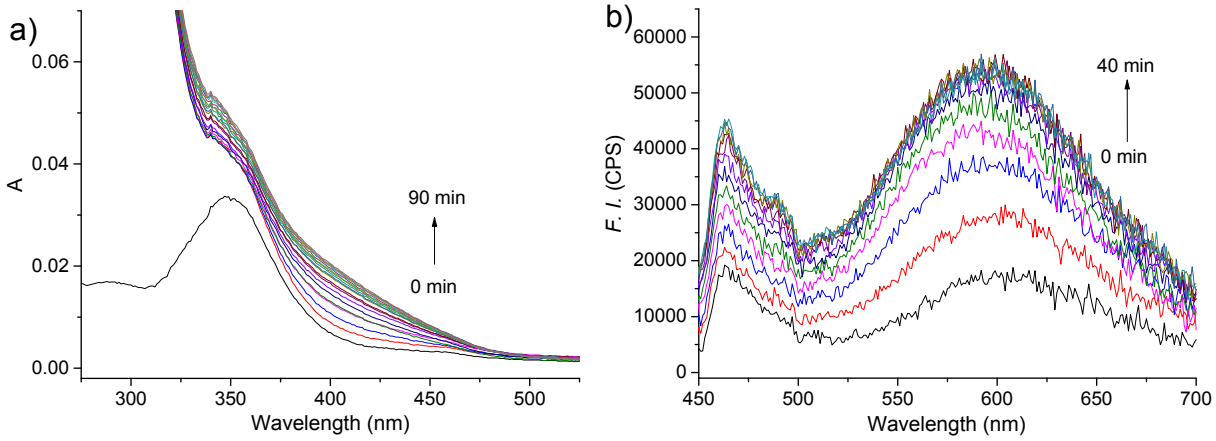

Figure S9 a) Time-dependent UV-Vis spectra of **NAP-DCP-4** (5 μM) and NOC-18 (1 mM) upon addition of 100 equiv. MGO at r. t.; b) Time-dependent fluorescence emission spectra (λ_{ex}=425 nm) of **NAP-DCP-4** (2 μM) and NOC-18 (1 mM) upon addition of 100 equiv. MGO at 37 °C.

3.8 3D fluorescence spectra studies of the probe NAP-DCP-4 (2 μM) before and after addition of 100 equiv. MGO for 1 h as well as further addition of 1000 equiv. NAC for 3 h

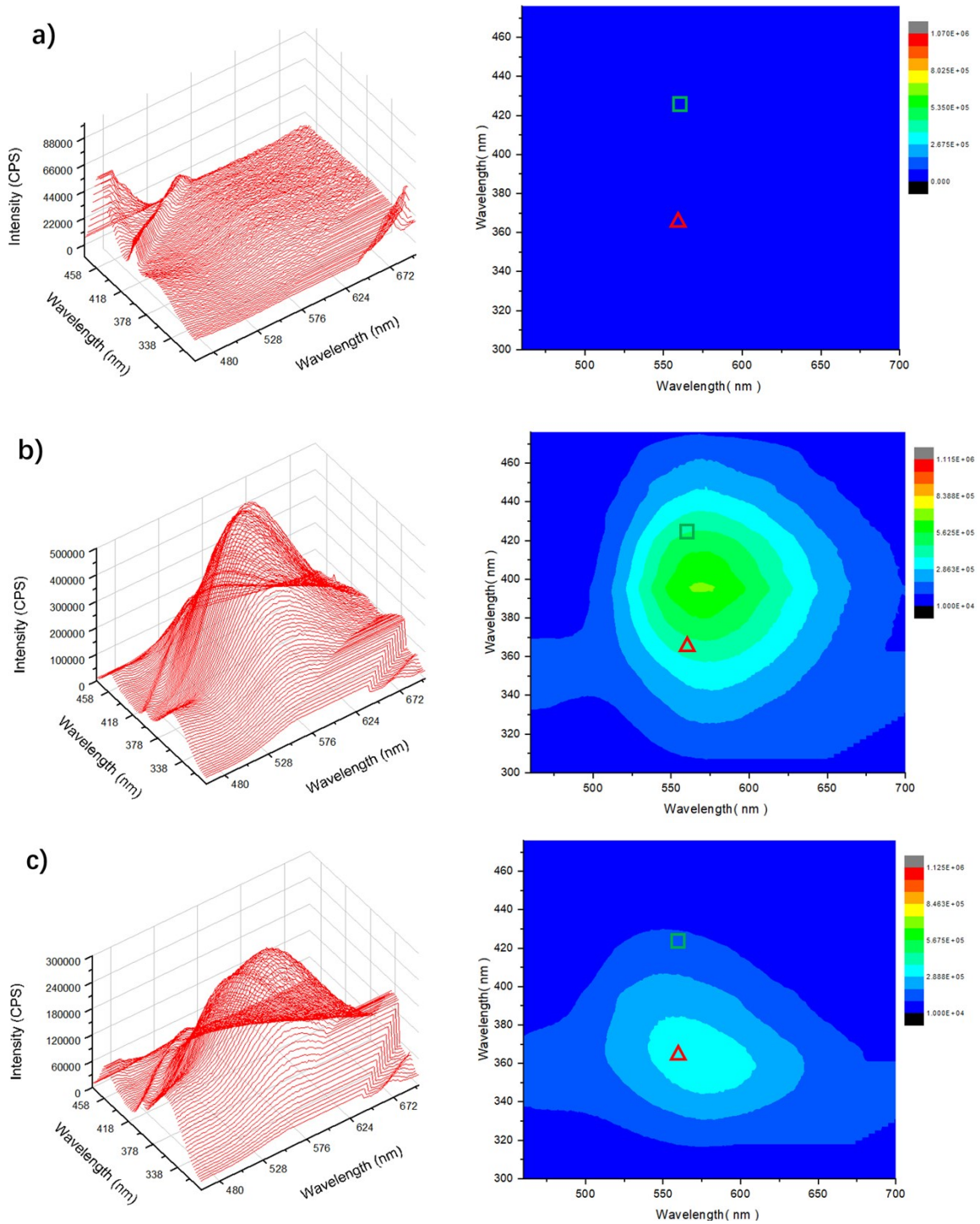

Figure S10 3D fluorescence spectra studies: a) the probe **NAP-DCP-4** (2 μM); b) the probe **NAP-DCP-4** (2 μM) incubated with 100 equiv. MGO for 1 h; c) the probe **NAP-DCP-4** (2 μM) incubated with 100 equiv. MGO for 1 h further treated with 1000 equiv. NAC for 3 h at 37 °C. (All measurements were performed in 10 mM PBS buffer at 37 °C, slit=5/5 nm, the fluorescent intensity at $\lambda_{ex/em}$=365/559 nm were marked by a red triangle, and the fluorescent intensity at $\lambda_{ex/em}$=425/559 were marked by a green square.) Clearly, the fluorescence intensity at both the triangle and the square positions gave fluorescence turn-on response for MGO. However, upon treated with NAC, the fluorescence turn-on response was reversed (reversible response) at the square position while it was remained (irreversible response) at the triangle position.

Part IV: Mass Spectrum Studies

4.1 HRMS studies of a reaction mixture of the probe NAP-DCP-4 and MGO in acetonitrile.

To a suspended solution of **NAP-DCP-4** (1.5 mg, 0.004 mmol) in 0.5 mL acetonitrile was added 7.8 equiv. MGO (40% MGO in H_2O, 5 μL). The mixture was stirred at 37 °C for 3 h to form a clear green solution. The solution was taken for HRMS analysis. The peak m/z 469.1638 was assigned to the $(M+H)^+$ peak of the bis-MGO adducts. The calculated value was 460.1619 (**Scheme S3**).

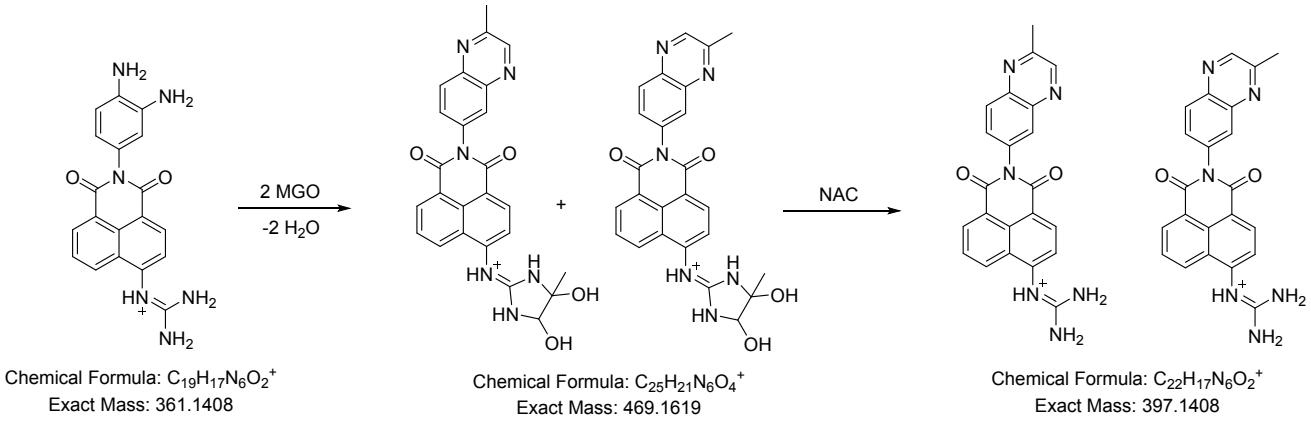

Scheme S3

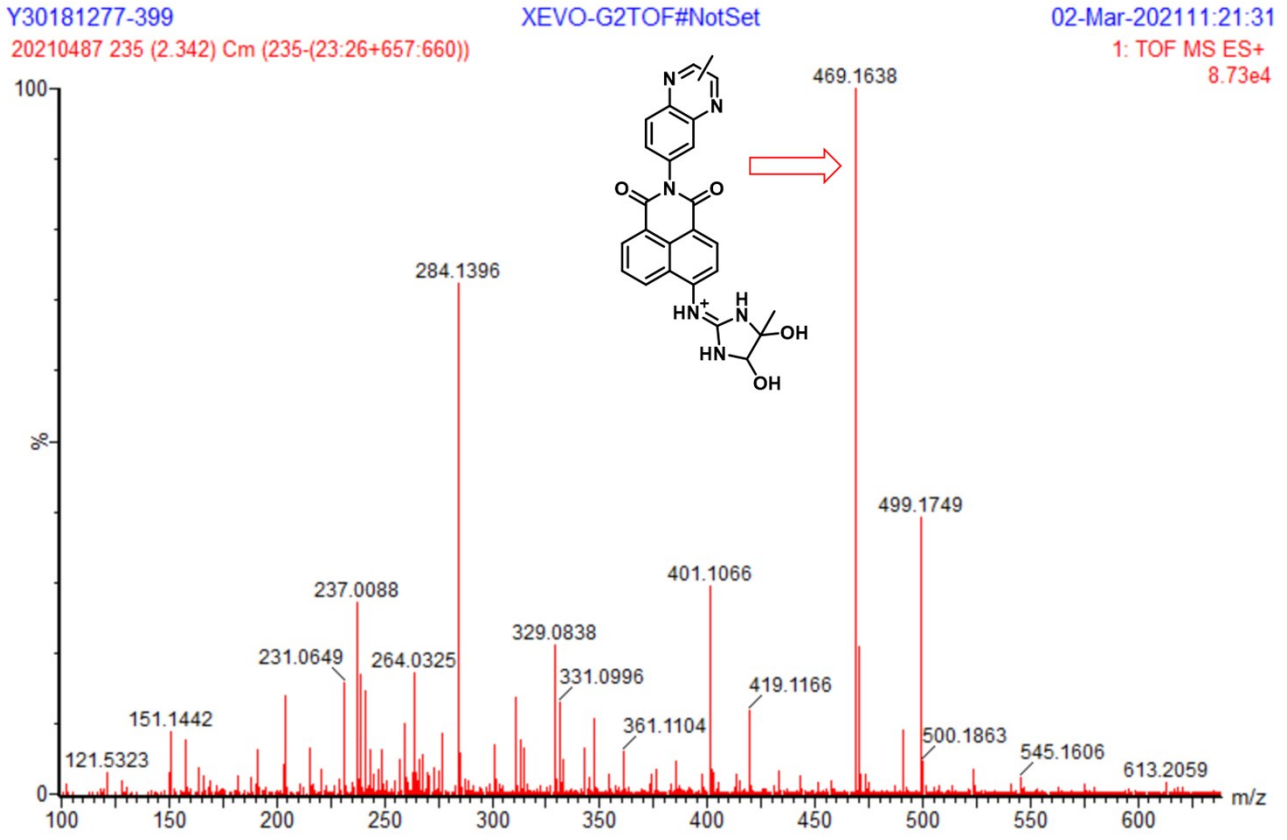

Figure S11 ESI-HRMS spectrum of the reaction mixture of **NAP-DCP-4** and **MGO**.

4.2 HRMS studies of a reaction equilibrium mixture of the probe NAP-DCP-4 and MGO in acetonitrile further addition of NAC.

To the above reaction equilibrium mixture of the probe **NAP-DCP-4** and MGO, was added NAC (48 mg, 0.29 mmol) and incubated at 37 ^{o}C for another 3 h. The solution was taken for HRMS analysis. The peak m/z 397.1414 was assigned to the $(M+H)^{+}$ peak of the mono-MGO adducts formed with the OPD reactive group. The calculated value was 397.1408 (**Scheme S3**).

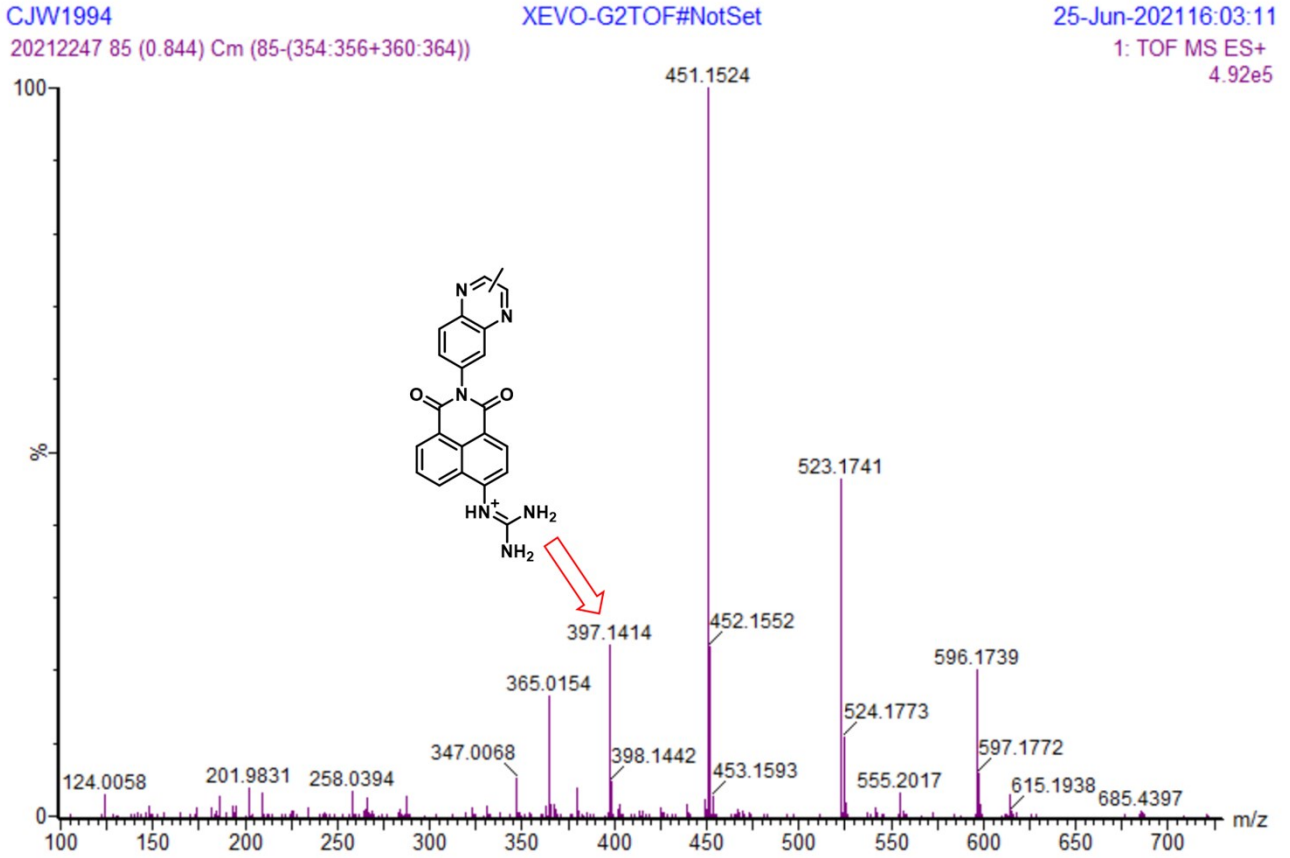

Figure S12 ESI-HRMS spectrum of the reaction equilibrium mixture of **NAP-DCP-4** and **MGO** treated with NAC.

Part V: Detection of Glyoxals in Live Cells

Cell culture: The murine macrophage RAW264.7 cell line was kindly provided by Stem Cell Bank, Chinese Academy of Sciences. RAW264.7 cells were maintained in DMEM medium (Gibco) supplied with 10% Fetal Bovine Serum (FBS, Gibco), 1% Glutamine (Gibco) and 1 mM Sodium Pyruvate at 37 °C in a humidified atmosphere containing 95% air and 5% CO_2.

LPS stimulation and MGO determination: One day before the experiment, RAW264.7 cells were seeded at 1 × 10^6 cells/mL in Nunc 6-well cell culture plates. In order to establish a hypoxia condition in the cell microenvironment, 200 μM $CoCl_2$ was added to the cells 4 h before the stimulation. Lipopolysaccharide (LPS) was diluted in cell culture medium and added to the wells at the final concentration of 100 ng/mL. *N*-acetyl cysteine (NAC) hydrochloride dissolved in cell culture medium and added to the wells at the final concentration of 5 mM. Cells were incubated for various amounts of time and cell/supernatant samples were collected at different time points. **NAP-DCP-4** probe was added to the samples on a PE OptiPlate Black 96-well microplate at 20 μM concentration and incubated for 1 h. Fluorescence intensity was measured on a SpectraMax i3x microplate reader (Molecular Devices) at excitation wavelength of 425 nm and the emission wavelength of 564 nm.

5.1 Cytotoxicity assay of the NAP-DCP-4

Cell survival was evaluated by the MTS assay (Promega CellTiter 96 AQueous One Solution Reagent, Cat No. G3582), based on the conversion of a tetrazolium compound, 3-(4,5-dimethylthiazol-2-yl)-5-(3-carboxymethoxy-phenyl)-2-(4-sulfophenyl)-2H tetrazolium (MTS), to a colored formazan product by living cells.[13] Absorbance was read by a microplate reader (BioTek Synergy Lx) at 490 nm. The quantity of formazan product, as measured by the amount of absorbance, was directly proportional to the metabolic activity of viable cells in the culture.

Cell viability (% of control) = $(OD_{EG}-OD_{ZG})/(OD_{CG}-OD_{ZG})*100\%$

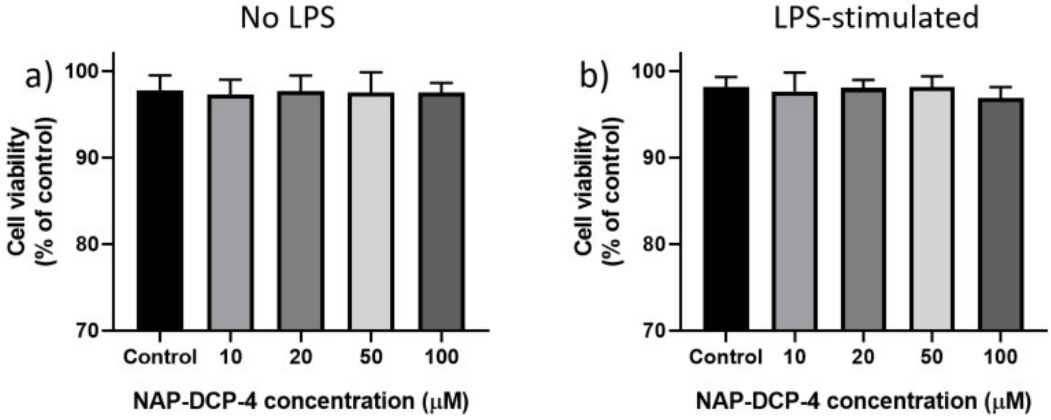

Figure S13 a) Cell viabilities of **NAP-DCP-4** at various concentrations for RAW264.7 cells after 24 h incubation; b) Cell viabilities of **NAP-DCP-4** at various concentrations for LPS-stimulated RAW264.7 cells after 24 h incubation.

5.2 Detection of MGO levels inside activated RAW264.7 cells

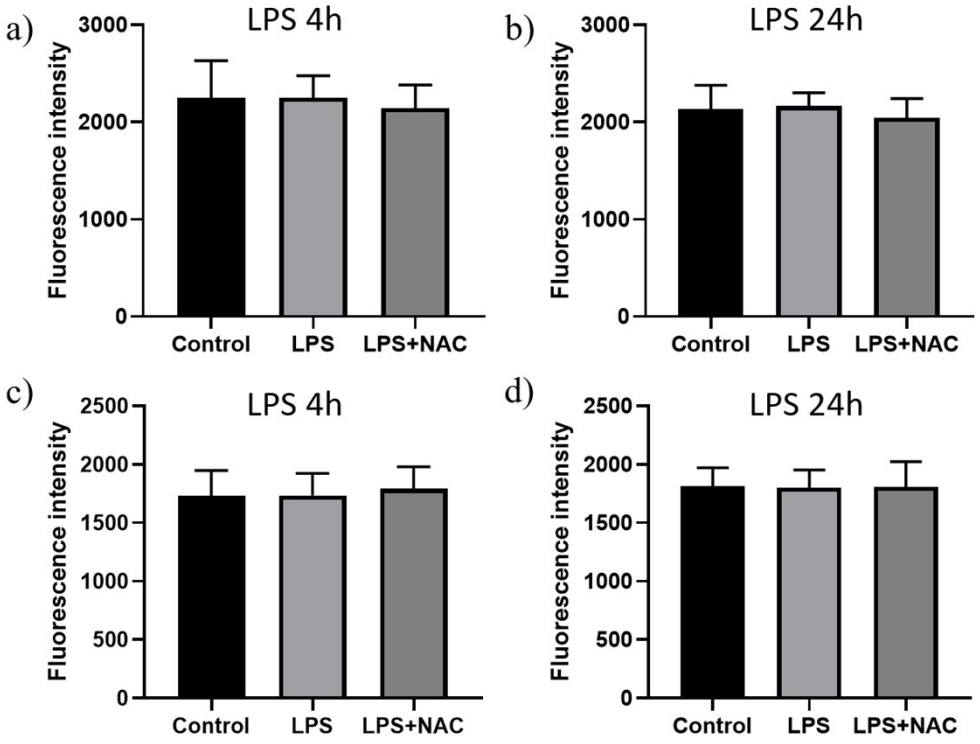

Figure S14 a) Fluorescence intensity of **NAP-DCP-4** in RAW264.7 cells stimulated with LPS for 4 h (λ_{ex}=425 nm); b) Fluorescence intensity of **NAP-DCP-4** in RAW264.7 cells stimulated with LPS for 24 h (λ_{ex}=425 nm); c) Fluorescence intensity of **NAP-DCP-4** in RAW264.7 cells stimulated with LPS for 4 h (λ_{ex}=365 nm); d) Fluorescence intensity of **NAP-DCP-4** in RAW264.7 cells stimulated with LPS for 24 h (λ_{ex}=365 nm).

5.3 Comparison of fluorescence Imaging of RAW264.7 cells with NAP-DCP-4 and NAP-DCP-1.

One day before the experiment, RAW264.7 cells were seeded at 1 × 10^6 cells/mL in Nunc 6-well cell culture plates to allow the cells to adhere. MGO was diluted in cell culture medium and added to the wells at the final concentration of 20 μM. After a 30 min incubation at 37 ℃, **NAP-DCP-4** and **NAP-DCP-1** were added to the different wells at 10 μM and the plates were incubated for another 30 min at 37 ℃. Cells were imaged without the washing step and fluorescence images were captured on a Nikon Eclipse Ti-S microscope equipped with 10× and 40× objective lens at Ex 450-490 nm/Em 540 nm.

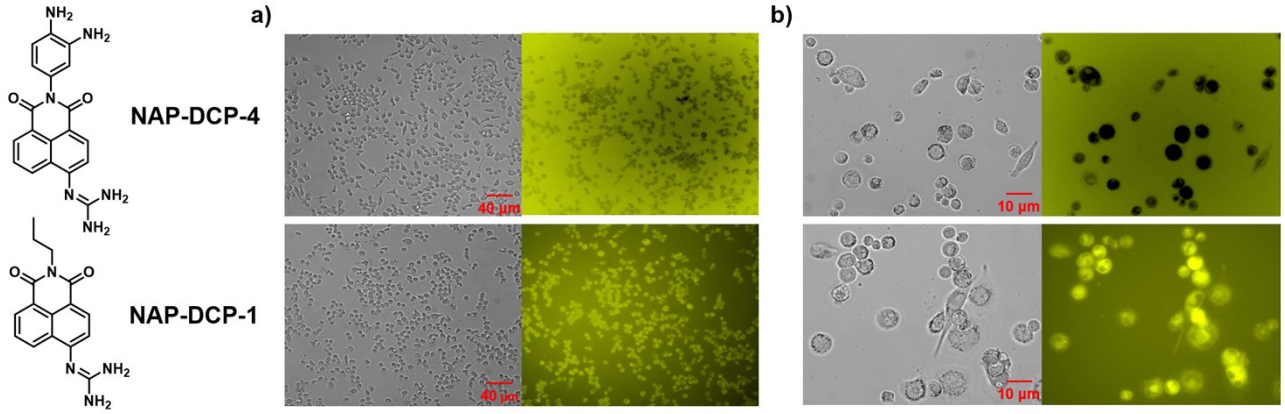

Figure S15 a) Bright field (left) or fluorescence (right) images of RAW264.7 cells incubated with 20 μM MGO and 10 μM **NAP-DCP-4** (up) or **NAP-DCP-1** (bottom) captured with 10× objective lens (scale bar = 40 μM). b) Bright field (left) or fluorescence (right) images of RAW264.7 cells incubated with 20 μM MGO and 10 μM **NAP-DCP-4** (up) or **NAP-DCP-1** (bottom) captured with 40× objective lens (scale bar =10 μM). A Nikon Eclipse Ti-S microscope was used for imaging (Ex 450-490 nm/Em 540 nm).

Part VIII: NMR and HRMS Data

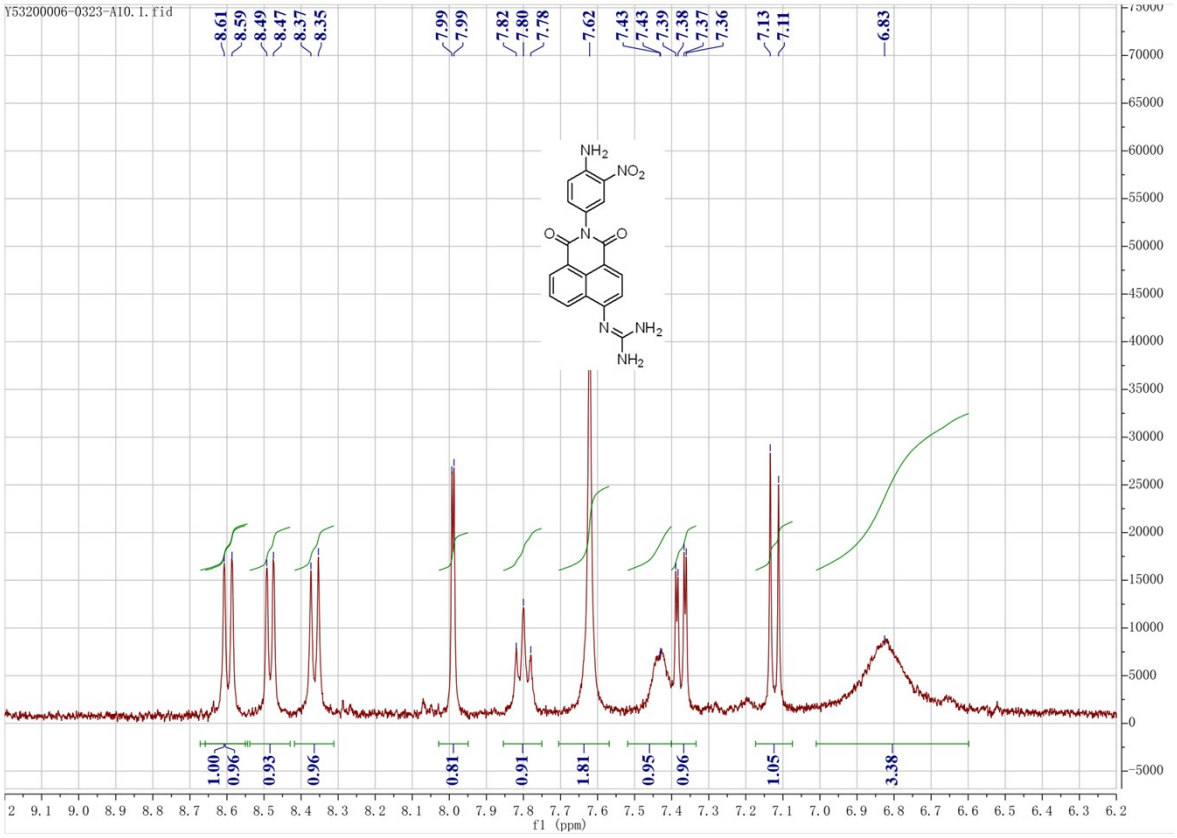

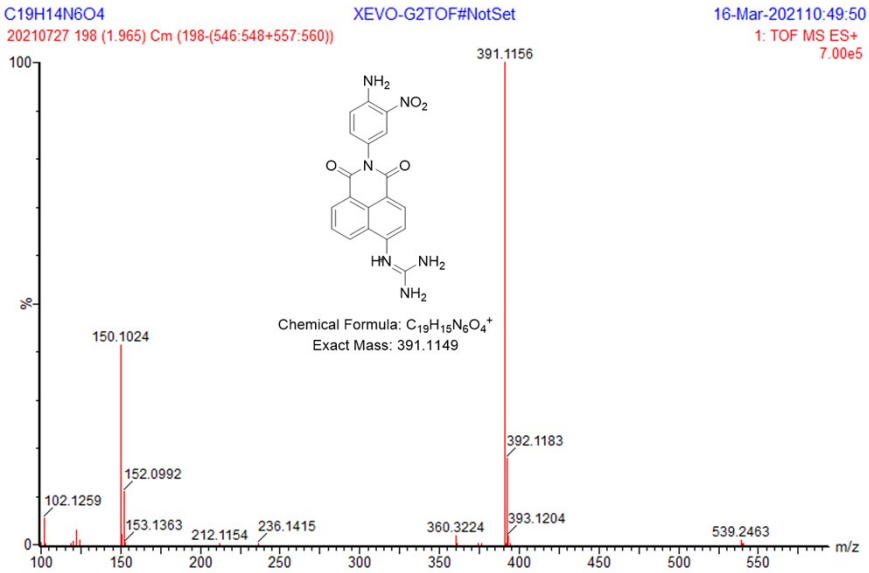

Figure S16 ^{1}H NMR and HRMS of the intermediate **5** (Due to its low solubility, satisfactory NMR spectra were difficult to obtain).

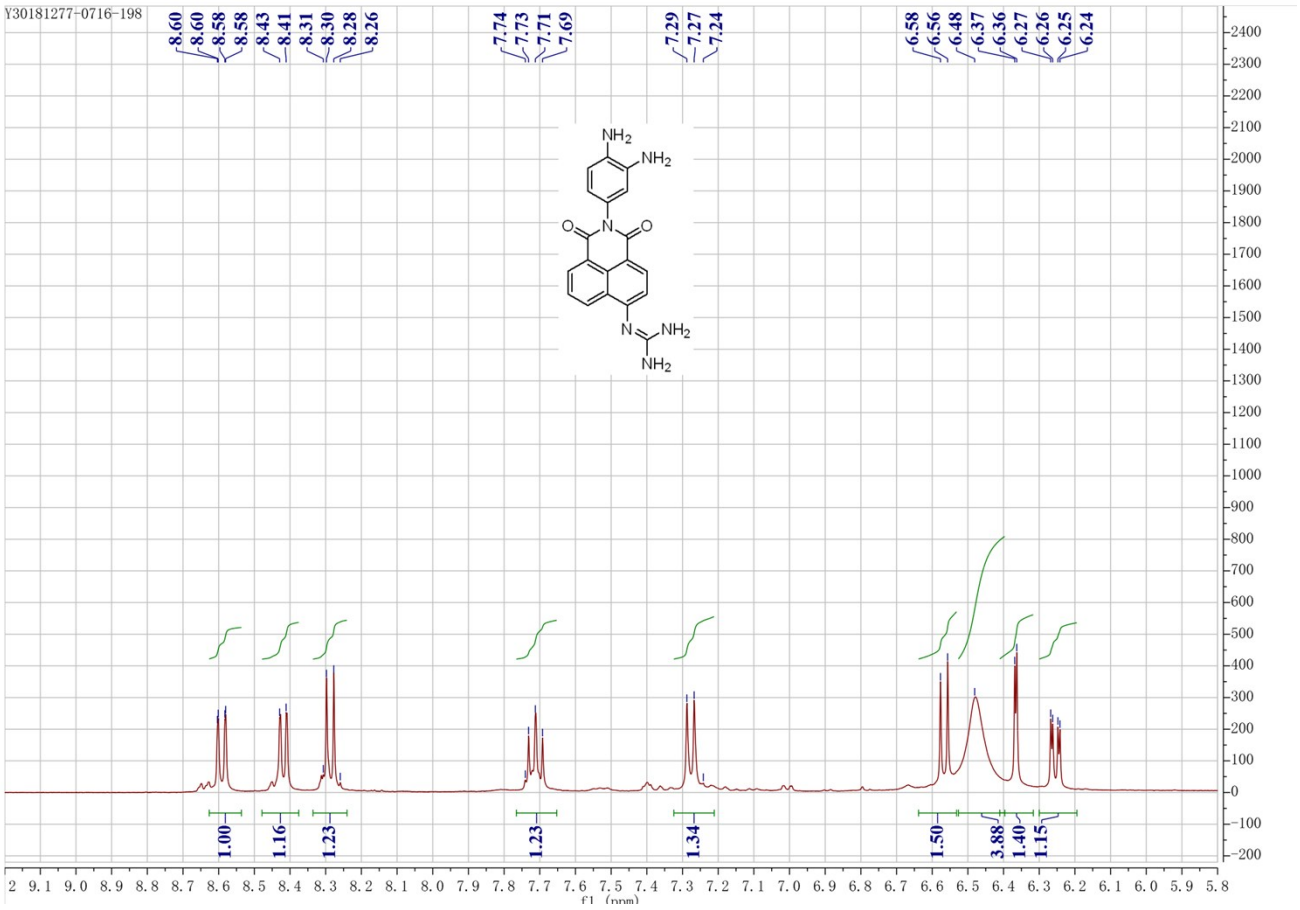
Y30181277-0716-198
8.60
8.60
8.58
8.58
8.43
8.41
8.31
8.30
8.28
8.26
7.74
7.73
7.71
7.69
7.29
7.27
7.24
6.58
6.56
6.48
6.37
6.36
6.27
6.26
6.25
6.24
NH2
NH2
O
N
O
N
NH2
NH2
1.00
1.16
1.23
1.23
1.34
1.50
3.88
1.40
1.15
f1 (ppm)

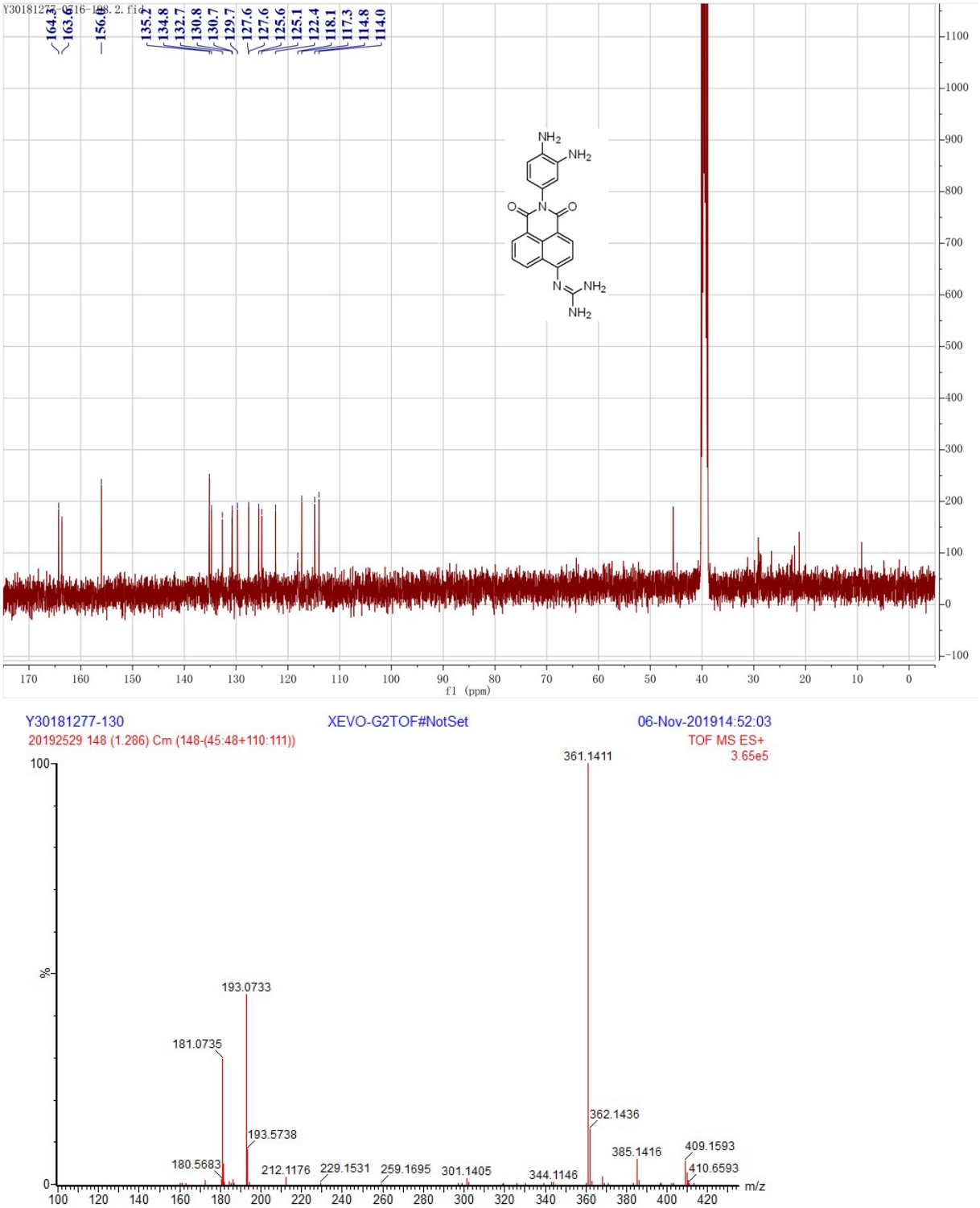

Figure S17 ^{1}H NMR, ^{13}C NMR, and HRMS of the probe **NAP-DCP-4**.

References

1. H. Wang, Y. Xu, L. Rao, C. Yang, H. Yuan, T. Gao, X. Chen, H. Sun, M. Xian, C. Liu and C. Liu, *Anal. Chem.*, 2019, **91**, 5646-5653.
2. M. Yang, J. Fan, J. Zhang, J. Du and X. Peng, *Chem. Sci.*, 2018, **9**, 6758-6764.

3. S. Gao, Y. Tang and W. Lin, *J. Fluoresc.*, 2019, **29**, 155-163.
4. T. Tang, Y. Zhou, Y. Chen, M. Li, Y. Feng, C. Wang, S. Wang and X. Zhou, *Anal. Methods*, 2015, **7**, 2386-2390.
5. T. Wang, E. F. Douglass, Jr., K. J. Fitzgerald and D. A. Spiegel, *J. Am. Chem. Soc.*, 2013, **135**, 12429-12433.
6. C. Liu, X. Jiao, S. He, L. Zhao and X. Zeng, *Dyes Pigm.*, 2017, **138**, 23-29.
7. F. Shaheen, A. Shmygol, N. Rabbani and P. J. Thornalley, *Biochem. Soc. Trans.*, 2014, **42**, 548-555.
8. C. Ding, F. Wang, Y. Dang, Z. Xu, L. Li, Y. Lai, H. Yu, Y. Luo, R. Huang, A. Zhang and W. Zhang, *Anal. Chem.*, 2019, **91**, 15577-15584.
9. Y. Dang, F. Wang, L. Li, Y. Lai, Z. Xu, Z. Xiong, A. Zhang, Y. Tian, C. Ding and W. Zhang, *Chem. Commun.*, 2020, **56**, 707-710.
10. W. Zhang, F. Zhang, Y.-L. Wang, B. Song, R. Zhang and J. Yuan, *Inorg. Chem.*, 2017, **56**, 1309-1318.
11. H. Xu, Q. Liu, X. Song, C. Wang, X. Wang, S. Ma, X. Wang, Y. Feng, X. Meng, X. Liu, W. Wang and K. Lou, *Anal. Chem.*, 2020, **92**, 13829-13838.
12. H. Yu, Y. Xiao and L. Jin, *J. Am. Chem. Soc.*, 2012, **134**, 17486-17489.
13. A. H. Cory, T. C. Owen, J. A. Barltrop and J. G. Cory, *Cancer Commun.*, 1991, **3**, 207-212.